Journal of Computational Physics 228 (2009) 7837–7849

Contents lists available at ScienceDirect

Journal of Computational Physics

journal homepage: www.elsevier.com/locate/jcp

A phase field model for vesicle–substrate adhesion ☆

Jian Zhang, Sovan Das, Qiang Du *

Department of Mathematics, Penn State University, University Park, PA 16802, USA

ARTICLE INFO

Article history:
Received 4 October 2008
Received in revised form 4 June 2009
Accepted 23 July 2009
Available online 3 August 2009

Keywords:
Vesicle
Adhesion
Elastic bending energy
Diffuse interface model
Phase field model
Adaptive finite element

ABSTRACT

In this paper, a phase field model is developed for vesicle adhesion involving complex substrate and vesicle geometries. The model takes into account an adhesion potential that depends on the distance of vesicle to the substrate. A variational problem is solved in a 3D computational domain by minimizing the contribution of bending elastic energy and the adhesion energy under the constraints of total surface area and volume, described via a phase function. An adaptive finite element method is used to efficiently compute the numerical solutions of the model. The computational results are validated through comparison of several axisymmetric shapes with the sharp-interface ODE solution. Moreover, we compute shapes for non-axisymmetric situations to support the observation that concave substrates favor adhesion.

1. Introduction

The Giant Unilamellar Vesicles (GUVs) made up by lipid bilayers have been used as a simplest model for cell membranes without the complexity of membrane bound proteins [23]. They permit the investigations of mechanistic and physicochemical aspects of cell membrane functions. One such function is adhesion which plays an important role in fundamental biological processes [1,17]. There have been much investigation on the adhesion of lipid bilayer vesicles to substrates which could lead to better understanding of the roles played by cell membrane in adhesion [24,30,33,35]. In this work, we develop a phase field approach for the adhesion of vesicles.

In a continuum mechanics description, the GUVs are modeled as two dimensional surfaces embedded in a three dimensional space [32], with their shapes being controlled mainly by the bending elastic energy. For isotropic membranes, the bending energy is formulated by the surface integral of the mean curvature square [20,32]:

$$E = \int_\Gamma c_1 H^2 ds, \tag{1}$$

where Γ is the vesicle surface, H is the mean curvature, and c_1 the bending modulus. During adhesion, the segment of a bound vesicle that interacts with the substrate can experience a variety of intramolecular forces [33] which thus gives rise to an effective adhesion potential $W(\mathbf{x})$ for any $\mathbf{x} \in \Gamma$. With such a consideration, the equilibrium vesicle–substrate adhesion model is given by minimizing the total energy functional

$$\mathcal{E}(\Gamma) = \int_\Gamma c_1 H^2 ds - \int_\Gamma W ds + \Sigma \int_\Gamma ds + p \int dV. \tag{2}$$

☆ The research is supported in part by NSF Grant DMS-0712744 and NIH Grant CA125707.
* Corresponding author. Tel.: +1 814 865 3674; fax: +1 814 865 3735.
E-mail addresses: zhang_j@math.psu.edu (J. Zhang), das@math.psu.edu (S. Das), qdu@math.psu.edu (Q. Du).

0021-9991/$ - see front matter © 2009 Elsevier Inc. All rights reserved.
doi:10.1016/j.jcp.2009.07.027

The quantities Σ and p correspond to the Lagrange multipliers for area and volume constraints, respectively, when the vesicle is assumed to conserve its surface area and enclosed volume during adhesion. In a recent study [11], we have investigated the influence of substrate geometry and curvature on the adhesion of vesicle, with the above form of bending elastic energy, in axisymmetric configurations. The contribution due to the Gaussian curvature has been ignored there, with the assumption that the vesicle does not change topology during adhesion.

In this paper, we extend our previously developed phase field diffuse interface models of vesicle membrane deformations to incorporate the effect of vesicle substrate adhesion as modeled by Eq. (2). The phase field model employs a diffuse interface description of the vesicle via a phase field function (order parameter) whose zero level set implicitly defines the vesicle surface Γ [13,14]. The phase field approach has the advantage that a single set of variational equations are defined in the whole computational domain without explicit reference to an interface. This in turn avoids complications in the design of numerical algorithms and provides a natural and systematic account for topology changes. For membrane deformation, this approach has become increasingly popular in the research community in recent years, we refer to [5,8,9,12–14,19,22,26,39] and the references cited therein.

To make a distinction in our presentation, the problem of finding the vesicle surface Γ to minimize the functional in (2) is referred as the sharp interface model. As the interfacial width parameter approaches to zero, the phase field model studied in this paper is consistent to (2). Due to the implicit surface representation of the vesicle, the phase field setting has the advantage of offering greater flexibility in the description of the contact domain (contact zone) with varying topology, which could not be easily addressed by the approach given in [11]. We further discuss an adaptive finite element method for the discretization of the phase field model. Some simulation results based on the adaptive FEM are reported to serve as the validation of both the consistency and the effectiveness of the phase field approach.

2. Discussion on the adhesion potential

There have been many studies on the various forms of adhesion energy between the vesicle and substrate. A particular popular form is modeled via an effective contact potential, that is

$$W(\mathbf{x}) = \begin{cases} w & \text{if} \quad d_s(\mathbf{x}) = 0, \\ 0 & \text{otherwise}, \end{cases} \tag{3}$$

with $d_s(\mathbf{x})$ being the distance of $\mathbf{x}$ to the prescribed substrate and w being a positive constant (here, the subscript s refers to the substrate in order to distinguish from the distance function to the interface Γ used later). Other forms such as the polynomial form [31], or the Morse potential [4] have also been introduced which provide an extra spatial length scale for which the adhesion effect is accounted for and are thus more realistic. As our purpose here is to introduce a general phase field framework that can take into account the adhesion energy which depends on the proximity of the vesicle with the substrate, we consider an adhesion potential W which has the form

$$W(\mathbf{x}) = w \exp(-d_s^2(\mathbf{x})/\delta^2), \tag{4}$$

with δ being a small parameter that determines the range of this potential. We refer to this as a Gaussian potential model due to the particular exponential form used. Notice that in the limit of $\delta = 0$, we effectively recover the contact area formula with the same w. As a verification of this consistency and an examination on how close the results are for small δ, we computed some three dimensional axisymmetric equilibrium shapes based on (3) and (4), respectively. As the parameter δ approaches zero, the solution with the contact area formula (3) is indeed recovered from the limit of the solutions corresponding to the Gaussian potential (4). The comparison of shapes are shown in Fig. 1 and the total bending energies and adhesion energies are provided in Table 1. The data corresponding to $\delta = 0$ refer to the results computed using the contact area formula.

The computation of the axisymmetric shapes with the contact potential is performed with a MATLAB code developed in [11] which handles only the case that the boundary of the contact area is given by a circle. The computation with the Gaussian potential is performed using similar techniques. We note that in the latter case, no assumptions are made on the vesicle being on one side of the substrate, thus, we see the slight protrusion of the vesicle surface into the substrate which are features associated with the use of Gaussian potential. Naturally, it might be unrealistic or less-physical if the protrusion starts to become significant. A geometric constraint can be explicitly imposed to eliminate the protrusion entirely should this become a significant issue. With proper choices of the initial profile and parameters, solutions with substantial protrusions have not been observed even without imposing the non-protrusion assumptions. Moreover, we note that other forms of the adhesion potential, such as the Morse potential would automatically prevent the protrusion because of the fact that the potential grows unbounded as the distance $d_s(\mathbf{x})$ approaches zero.

3. A phase field formulation

For the sharp-interface model, the investigation in the axisymmetric configuration reduced the Euler–Lagrange equations to a system of ordinary differential equations (ODEs) similar to the analysis given in [11]. These ODEs can thus be solved easily using an ODE solver for boundary value problems. In order to study more general substrates and vesicle shapes, we need to work with the more general form of the Euler–Lagrange equations which consist of a set of highly-nonlinear partial

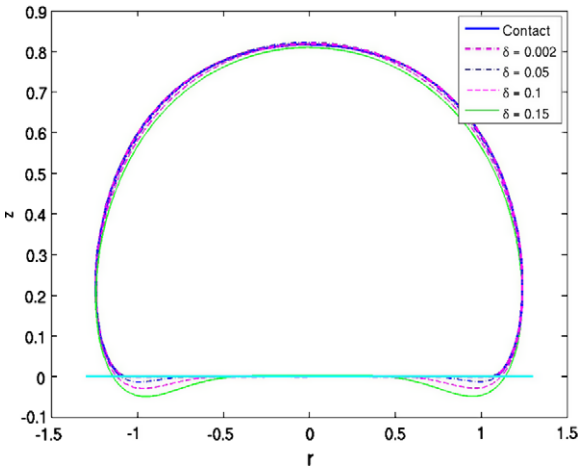

Fig. 1. Convergence of shapes for the Gaussian potential with $w = 10$ for values of $\delta \to 0$, the limiting shape corresponds to a contact potential with the same w.

Table 1
The bending and adhesion energies for the shapes shown in Fig. 1.

Energy/δ	0.15	0.10	0.05	0.002	0.0
Bending energy	21.259	21.824	22.977	25.767	26.149
Adhesion energy	45.043	43.645	41.340	36.366	34.934

differential equations. By now, a number of techniques have been developed to numerically approximate such equations, including widely-known methods in discrete computational geometry, immersed boundary approach and more recently proposed methods based on finite element modeling [2,6,18,25,27,29]. In the current work, we adopt the phase field approach which has been developed to model the vesicle deformation and interactions with various external fields [13,12]. Using a diffuse interface description of the vesicle surface, the phase field model for adhesion is a natural extension of the phase field model developed in our earlier works for the vesicle deformations. It provides great flexibility in describing the vesicle deformation as well as the change of contact geometry. It also represents another step forward in building up a phase field framework for modeling the complex morphologies and interactions of vesicle membrane with other biological entities and physical environment.

We now introduce a phase function $\phi = \phi(\mathbf{x})$ defined on the physical (computational) domain Ω that is taken to be large enough to enclose both the vesicle and the part of substrate of interest. The function ϕ is used to label the inside and the outside of the vesicle Γ so that the level set $\{\mathbf{x} : \phi(\mathbf{x}) = 0\}$ gives the membrane, while $\{\mathbf{x} : \phi(\mathbf{x}) > 0\}$ represents the inside of the membrane and $\{\mathbf{x} : \phi(\mathbf{x}) \leqslant 0\}$ the outside. As in our earlier works, we define the following phase field form of the bending elastic energy:

$$E_\epsilon(\phi) = \int_\Omega \frac{3\sqrt{2}c_1\epsilon}{16}\left(\Delta\phi - \frac{1}{\epsilon^2}(\phi^2 - 1)\phi\right)^2 d\mathbf{x}, \tag{5}$$

where ϵ is a *transition* parameter that characterizes the width of the diffuse interfacial layer and is taken to be very small compared to the size of the vesicle. The functional E_ϵ is defined as the bulk integrals on the whole domain, rather than the surface integrals as those in (1). Such energetic formulations may be viewed as diffusive relaxations or approximations of the sharp interface models as they induce a thin transitional region near the interface and the parameter ϵ represents the thickness of this region.

For the adhesion energy, we adopt a corresponding phase field formulation

$$\int_\Omega W(\mathbf{x})F_\epsilon(\phi(x), \nabla\phi(x))d\mathbf{x},$$

where $F_\epsilon(\phi, \nabla\phi)$ is a function of the phase field variable ϕ with the property that for small ϵ,

(1) it is non-negative everywhere;
(2) its value approaches to zero for $\mathbf{x}$ outside the diffuse interfacial layer;
(3) its integral over the domain Ω is close to 1.

These conditions naturally imply that $F(\phi, \nabla\phi)$ should act like a measure concentrated in the diffuse interfacial layer surrounding the 0 level set of ϕ. Given the understanding that the phase field variables, especially those with bounded bending energies as analyzed in [12,38], are nearly ±1 inside and outside the vesicle, with a typical tanh-like profile, it is possible to construct several possible forms such as

$$\frac{3\sqrt{2}\epsilon}{4}|\nabla\phi|^2, \quad \text{or} \quad \frac{3\sqrt{2}}{4}\left[\frac{\epsilon}{2}|\nabla\phi|^2 + \frac{(\phi^2-1)^2}{4\epsilon}\right],$$

to meet the above conditions. In the current paper, for simplicity, we elect to take

$$F_\epsilon(\phi, \nabla\phi) = \frac{3\sqrt{2}}{8}\frac{(\phi^2-1)^2}{\epsilon}. \tag{6}$$

For the volume and surface area constraints, we define the associated phase field functionals:

$$A(\phi) = \int_\Omega \frac{\phi(\mathbf{x})+1}{2} d\mathbf{x}, \tag{7}$$

and

$$B(\phi) = \frac{3\sqrt{2}}{4}\int_\Omega \left[\frac{\epsilon}{2}|\nabla\phi|^2 + \frac{1}{4\epsilon}(\phi^2-1)^2\right] d\mathbf{x}. \tag{8}$$

We note that the phase field framework developed above can be extended to incorporate other physically and biologically interesting features as well. For instance, following the study in [21], a gravitational energy due to the density difference between the fluid inside and outside the vesicle can also be considered when the vesicle is relatively large. A gravitational potential of the form

$$G\int_\Omega \frac{1-\phi}{2} x_3 d\mathbf{x}, \tag{9}$$

can be included in the total energy in the phase field setting, where G is a dimensionless gravity parameter and $\mathbf{x} = (x_1, x_2, x_3)$ with x_3 denoting the height of a volume element. Given the fact that the phase function ϕ is nearly 1 outside the vesicle and nearly -1 inside, in the sharp interface limit, this potential approaches $G\int x_3 d\mathbf{x}$ which is consistent to the form considered in [21].

To summarize, by using the penalty formulation for the volume and surface area constraints, the total energy in the phase field form is then given by

$$\begin{aligned}\mathcal{E}_\epsilon(\phi) = {} & \int_\Omega \frac{3\sqrt{2}c_1\epsilon}{16}\left(\Delta\phi - \frac{1}{\epsilon^2}(\phi^2-1)\phi\right)^2 d\mathbf{x} - \int_\Omega \frac{3\sqrt{2}}{8}W(\mathbf{x})\frac{(\phi^2-1)^2}{\epsilon} d\mathbf{x} + G\int_\Omega \frac{1-\phi}{2}x_3 d\mathbf{x} + M_1(A(\phi)-\alpha)^2 \\ & + M_2(B(\phi)-\beta)^2.\end{aligned} \tag{10}$$

The original problem of minimizing the bending elastic energy, adhesion energy and gravitational energy with the prescribed surface area and volume is now effectively transformed into the problem of finding, for small ϵ, the function $\phi = \phi(\mathbf{x})$ on the entire three dimensional computational domain that minimizes the energy $\mathcal{E}_\epsilon(\phi)$. The parameters α and β now prescribe the values of the constraint functionals A and B associated with the volume and surface area, respectively.

The solution of the minimizing problem satisfies the Euler–Lagrange equation of the energy functional $\mathcal{E}_\epsilon(\phi)$ which, in the weak form, is given by:

$$-\frac{3\sqrt{2c_1\epsilon}}{8}\int_\Omega \left[\nabla f\cdot\nabla v + \frac{1}{\epsilon^2}f(3\phi^2-1)v\right] d\mathbf{x} - \frac{3\sqrt{2}}{2\epsilon}\int_\Omega W(\mathbf{x})(\phi^2-1)\phi v d\mathbf{x} + \int_\Omega \left(\lambda - \frac{3\sqrt{2\epsilon}}{4\sqrt{c_1}}\mu f - \frac{G}{2}x_3\right) v d\mathbf{x} = 0,$$

for any suitably defined test function v, where

$$\lambda = 2M_1[A(\phi)-\alpha], \quad \mu = 2M_2[B(\phi)-\beta],$$

and

$$f = \sqrt{c_1\epsilon}\left[\triangle\phi - \frac{1}{\epsilon^2}(\phi^2-1)\phi\right].$$

The last equation can also be written in the weak form as

$$\sqrt{c_1\epsilon}\left[\int_\Omega \nabla\phi\cdot\nabla u + \frac{1}{\epsilon^2}\int_\Omega (\phi^2-1)\phi u d\mathbf{x}\right] + \int_\Omega f u d\mathbf{x} = 0.$$

for any suitably defined test function u. Note that either Dirichlet boundary condition or natural boundary conditions can be specified. Following similar analysis as that in [15], it can be shown that as M_1 and M_2 go to infinity, λ and μ converge to the Lagrange multipliers corresponding to the Eqs. (7) and (8).

Intuitively, it is insightful to consider a special phase field function of the form $\phi(\mathbf{x}) = \tanh\left(\frac{d(\mathbf{x},\Gamma)}{\sqrt{2}\epsilon}\right)$ where $d(\mathbf{x},\Gamma)$ is the signed distance from a point $\mathbf{x} \in \Omega$ to the surface Γ. In such an ansatz, it can be readily seen that, as ϵ approaches to zero, $A(\phi)$ approaches the difference of the volume outside and inside the vesicle and $B(\phi)$ approaches the surface area, while the phase field forms of the bending elastic energy and the adhesion energy approach to the sharp interface version given by (1) and (4). A more rigorous analysis of the consistency between the phase field model and the sharp interface model can be given based on the similar analysis presented in [12,38] under the assumption of a more general ansatz. We leave out the details in the current study.

While the phase field approach allows the capturing of vesicles with more complex topology and more general contact geometry using a single set of differential equations in the whole computational domain, it appears to require much more computational cost in comparison with the sharp interface description used for the axisymmetric analysis. This is because of the increase in the dimension, that is, the determination of the phase field function is through solving the system of differential equations corresponding to the Euler–Lagrange equations defined in the three dimensional domain Ω, even though we are mostly interested in the two dimensional zero level set of the phase field function corresponding to the vesicle surface Γ. To reduce the computational overhead, we employ an adaptive finite element method to compute the solutions of the phase field model so that most of the computational grids are mainly concentrated near the vesicle surface [16]. Away from the vesicle surface, the phase field function is nearly ±1 with very small spatial derivatives so that a coarse mesh can be used without incurring significant loss of accuracy. The details are given in the next section.

4. Numerical methods for the phase field model

In our earlier works, we have developed a number of strategies to numerically solve the phase field bending energy models. These include the finite difference methods [13], Fourier spectral methods [14], and finite element methods [16]. Here, we adopt the adaptive finite element approximation developed in [16] based on a suitably defined residual type a posteriori error estimator.

4.1. An adaptive FEM

We now present a brief account of the adaptive finite element method based on a conforming mixed finite element approximation on a three dimensional isotropic tetrahedral mesh. For a detailed discussion, we refer to [16] and the references therein. We first construct a conforming C^0 finite element space V^h defined with respect to a triangulation of the computational domain Ω. Here, h is simply used as a notation for the mesh. The constructed tetrahedral meshes are assumed to be uniformly regular so that the standard maximum and minimum angle conditions are satisfied and the number of adjacent elements to any given element is bounded independently of the mesh as the mesh gets refined.

Based on the weak formulation of the Euler–Lagrange equations and the definition of f, we have the following mixed formulation for the approximate finite element solution ϕ_h and f_h in a trial conforming C^0 finite element space V^h:

$$\begin{cases} -\frac{3\sqrt{2c_1}\epsilon}{8}\left[\int_\Omega \nabla f_h \cdot \nabla v_h d\mathbf{x} + \frac{1}{\epsilon^2}\int_\Omega f_h(3\phi_h^2-1)v_h d\mathbf{x}\right] + \lambda_h \int_\Omega v_h d\mathbf{x} \\ -\frac{3\sqrt{2}}{2\epsilon}\int_\Omega W(x)(\phi_h^2-1)\phi_h v_h d\mathbf{x} - \frac{3\sqrt{2\epsilon}}{4\sqrt{c_1}}\mu_h \int_\Omega f_h v_h d\mathbf{x} - \frac{G}{2}\int_\Omega x_3 v_h d\mathbf{x} = 0, \\ \sqrt{c_1\epsilon}\left[\int_\Omega \nabla\phi_h \cdot \nabla u_h d\mathbf{x} + \frac{1}{\epsilon^2}\int_\Omega(\phi_h^2-1)\phi_h u_h d\mathbf{x}\right] + \int_\Omega f_h u_h d\mathbf{x} = 0, \end{cases} \tag{11}$$

for all test functions v_h, u_h in the corresponding finite element test function space. ϕ^h is also assumed to satisfy the constraints (7) and (8) and λ_h and μ_h are the corresponding Lagrange multipliers. Again, boundary conditions are properly enforced either in the definition of the finite element spaces or in the approximate weak forms.

Finite element solutions can be obtained by either solving the nonlinear algebraic systems given by (11), or via a direct optimization process of the discretized form of the phase field energy functional. In the phase field models, for small (and constant) interfacial width ϵ, the phase field solutions display large gradients within the diffusive interfacial region. Thus, mesh adaptivity in the form of mesh-refinement and coarsening as well as mesh transformation can greatly improve the efficiency of the numerical approximations. A posteriori error estimators are key ingredients in the design of adaptive methods [3]. There have been many existing studies on deriving such estimators for the finite element approximation of linear and nonlinear variational problems and for standard Galerkin and mixed finite element formulations, see for example [10,37] and the references cited therein. In our earlier works, we reported the use of a residual type a posteriori error estimators derived from the Eq. (11) in the absence of the adhesion energy term. A similar estimator can be derived to account for the contribution of the adhesion potential term as well, and it has the form:

$$\eta_K = \left\{ \left[\frac{3\sqrt{2c_1}\epsilon}{8} \sum_{e\subset\Omega\cap\overline{K}} h_e^{\frac{1}{2}}|e|^{\frac{1}{2}} \left\| \left[\frac{\partial f_h}{\partial n}\right]_e \right\| + h_K \left\| \lambda_h - \frac{G}{2}x_3 - \frac{3\sqrt{2c_1}}{8\sqrt{\epsilon^3}} f_h(3\phi_h^2-1) - \frac{3\sqrt{2}}{2\epsilon}W(x)(\phi_h^2-1)\phi_h - \frac{3\sqrt{2\epsilon}}{4\sqrt{c_1}}\mu_h f_h \right\|_K \right]^2 \right.$$
$$\left. + C^2 \left[\sqrt{\epsilon} \sum_{e\subset\Omega\cap\overline{K}} h_e^{\frac{1}{2}}|e|^{\frac{1}{2}} \left\| \left[\frac{\partial \phi_h}{\partial n}\right]_e \right\| + h_K \left\| f_h + \frac{\sqrt{c_1}}{\epsilon^{3/2}}(\phi_h^2-1)\phi_h \right\|_K \right]^2 \right\}^{\frac{1}{2}}, \tag{12}$$

on a tetrahedron K with $|e|$ being the area of one of its face e, h_K and h_e being the corresponding mesh parameters of the tetrahedral element K and the face e. The constant C is a weight coefficient used to balance the needs for resolving the thin interfacial layer and the curvature of the vesicle.

The adaptive algorithm based on the above error estimator is similar to the one adopted in [16] with the objective of reducing the error effectively to a given error tolerance. Briefly, let $\{M_j\}_{j\geqslant 0}$ represent the various level of meshes generated from the refinement and coarsening procedure and *tol* be a specified error tolerance. We introduce two parameters $r_f > 1 > c_f$ as the so called *refine factor* and *coarsen factor*. Then, following similar procedures documented in [16], the general adaptive algorithm is given by the steps below:

Algorithm 4.1. Adaptive FEM

Start with mesh M_0, *set* $j := 0$; $\eta := tol + 1$.
  while $\eta > tol$, *do*
    solve the discrete problem on M_j;
    compute local and global error indicators $\{\eta_K\}$ *and* $\eta = \{\sum_K \eta_K^2\}^{\frac{1}{2}}$;
    if $\eta > tol$, *let N be the number of elements in* M_j;
      for all element K, do
        if $\eta_K > r_f\eta/\sqrt{N}$, *mark K for refinement, end if;*
        if $\eta_K < c_f\eta/\sqrt{N}$, *mark K for coarsening, end if;*
      end for;
      update M_j *to get* M_{j+1} *and set* $j := j + 1$;
    end if;
  end while.

Based on our experience [16], we used $r_f = 1.4$ and $c_f = 0.7$ in our simulations. For elements to be marked for coarsening, the step only takes place if the resulting mesh remains conforming.

The reliability and effectiveness of the above adaptive algorithm have been carefully examined in [16] for the case without the adhesion energy. Our simulation indicates that the effectiveness is maintained with the additional terms. The detailed analytical works are omitted but the numerical illustrations are provided in the next section.

4.2. The computation of finite element solutions on a given mesh

In the numerical implementation, we work with a minimization procedure to solve for the finite element approximations on adaptive meshes. For a given mesh, the minimization of E is carried out using a gradient flow approach [13,15]. Using a backward Euler scheme for the gradient flow, we again arrive at a variational problem of minimizing the functional

$$\frac{1}{2}\frac{\|\phi_{n+1} - \phi_n\|^2}{\Delta t_n} + \mathcal{E}_\epsilon(\phi_{n+1}), \tag{13}$$

with the constraints being enforced as penalty terms. The solution of (13) at each step is obtained using the nonlinear Conjugate Gradient (NCG) iterative solver with a diagonal preconditioner. For small Δt_n, the diagonal matrix is dominated by the contribution of entries in the mass matrix which scale proportionally with the element size. The diagonal preconditioning thus counter-balances the large variations in the matrix entries due to the adaptive meshing and helps to accelerate the convergence of the NCG iteration. We generally adjust the time step Δt_n so that the NCG method converges in 20–40 steps. This allows efficient computation at each time step.

4.3. Choice of parameters and initialization

Without loss of generality, the computational domain Ω was taken to be a cube of the size $[-1.5, 1.5]^3$, with the vesicle take up a sizable proportion of the domain. The bending rigidity was taken to be $c_1 = 1$.

We took the penalty constants large enough so that the volume and surface area constraints are satisfied with less than 0.5% error. Computationally, we find that it suffices to take $M_1 = 10,000$ and $M_2 = 10,000$. We numerically verified the convergence of the Lagrange multipliers with such choices of penalty constants.

In practice, ϵ is taken to be a very small number so that the thickness of the diffusive interfacial layer is much less than the size of the vesicle and the range of the interaction between the vesicle and the substrate.

In some of our numerical examples, the parameter δ used in the Gaussian potential is taken to be $\delta = 0.15$. To get an idea about how small an ϵ would suffice, we performed some tests on a vesicle adhering to a flat substrate. The results, given in the next section, show that one can get satisfying approximation of the adhesion energy when ϵ equals 0.04. Thus, depending on the accuracy requirement, we typically keep ϵ, in our numerical examples, in the range between 0.02 and 0.04. Based on the extensive numerical tests in [16], with ϵ in this particular range, $C = 100$ is seen as a good choice for the coefficient used in the a posterior error estimator.

The choice of initial profiles also plays an important role in the performance of the numerical optimization routine. We typically used a *tanh* profile associated with a particular candidate interface as the initial guess for the phase field function. Since no explicit assumptions on the protrusion of the vesicle onto the substrate have been given, it is customary to make the candidate initial interface situated on one side of (say, above) the substrate. Computationally, this ensures that the captured vesicle surface would largely stay on one side of the substrate with the size of the protrusion well within diffuse interface layer.

5. Numerical examples

We now present some numerical examples based on the adaptive finite element approximations to the phase field formulations. Since the quantitative assessment on the performance of the adaptive finite element method for the phase field bending energy model has already been well documented in [16], we hereby mostly focus on validating the phase field approach and demonstrating its effectiveness in modeling the vesicle substrate adhesion. Note that the effect of the gravity is only considered in the final example, and for other examples, the gravity term is not included.

5.1. Comparison with sharp interface solution

We first design a series of tests on assessing the accuracy of the phase field energy (10) to the sharp interface energy (2). Since the sharp interface model is best solved for axisymmetric case using the developed ODE solver, we take an axisymmetric case as an illustration.

In order to obtain good resolution of the vesicle curvature, the effective thickness of the interfacial layer of ϕ is set to be 2% of the size of the vesicle which requires us to take $\epsilon = 0.04$. We choose a flat substrate at $z = 0$ with the interaction range

Table 2
Comparison of elastic bending and adhesion energies computed by sharp interface (SI) and phase field (PF) methods.

Energy	Method	$w = 1$	$w = 2$	$w = 5$	$w = 10$
Bending	SI	20.97	21.15	21.91	23.20
Bending	PF	21.40	21.51	22.55	24.17
Adhesion	SI	−4.66	−9.59	−25.15	−52.13
Adhesion	PF	−4.61	−9.50	−24.95	−52.03

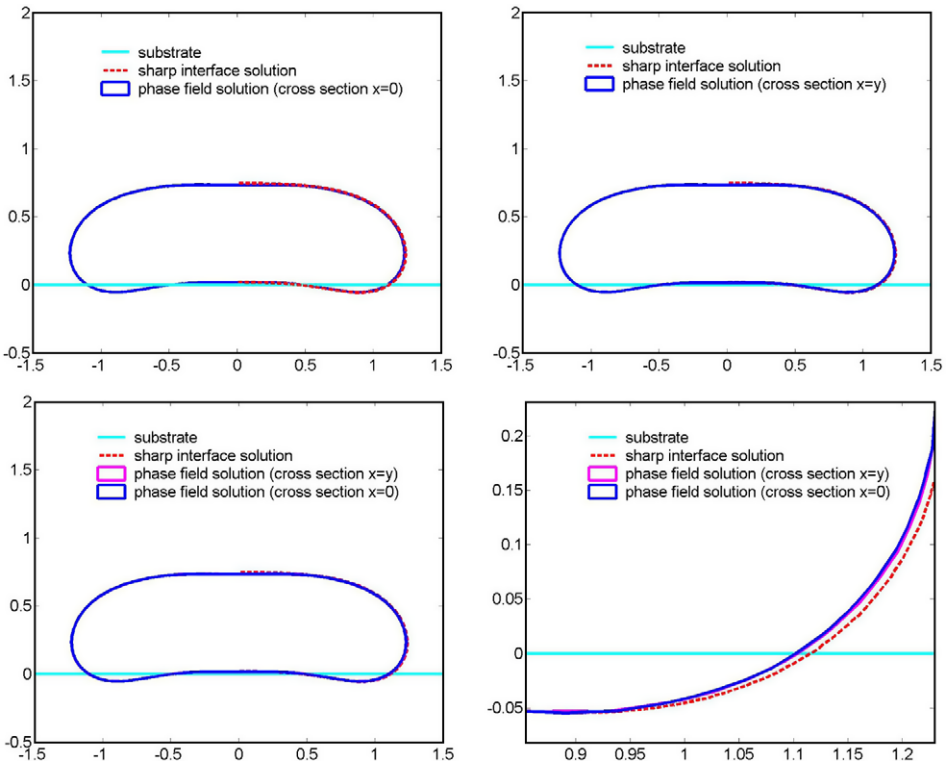

Fig. 2. Comparisons of different cross sections of solutions for $w = 5, \delta = 0.15$ and $\epsilon = 0.04$. The phase field computation does not assume axisymmetry but the solution remains fairly axisymmetric. An enlarged area around the high curvature points is also shown.

parameter $\delta = 0.15$ in the Gaussian potential. An axisymmetric vesicle is used as a bench-mark. The energies of the solutions of the phase field model are compared with those for the sharp interface model for different values of w. The sharp interface model is solved using an ODE solver as described in [11] and the solution is used to generate a rough initial profile for the phase field computation. The phase field model then is solved using the adaptive FEM. The resulting bending and adhesion energies are listed in Table 2. We can see that for this range of w, the adhesion energy values display significant variations in comparison with those of the bending energy. In fact, the adhesion energy changes, in absolute value, from being a relatively small percentage (less than 25%) of the bending energy, to being more than twice the bending energy.

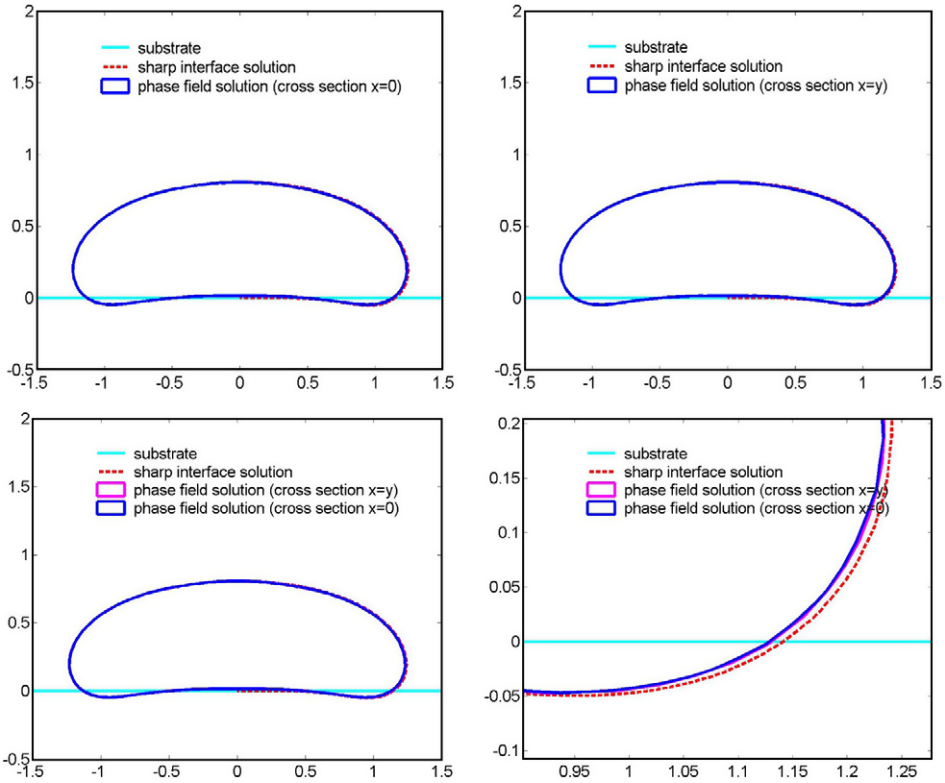

Fig. 3. Comparisons of different cross sections of solutions for $w = 10, \delta = 0.15$ and $\epsilon = 0.04$. Enlarged area near the high curvature points around $(x, y) = (1, 0)$ is also shown. With no assumption on the vesicle being on one side of the substrate, a slight protrusion of the vesicle surface into the substrate is observed.

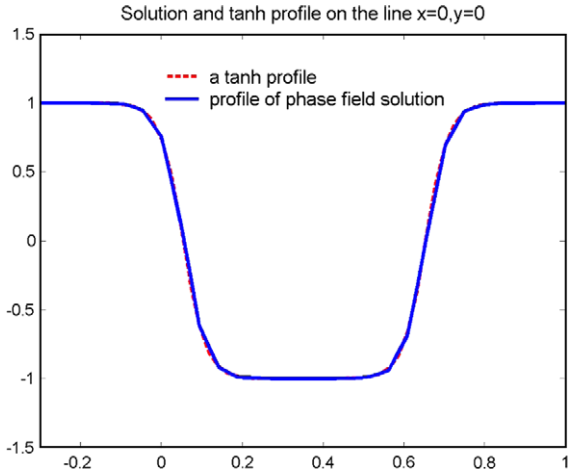

Fig. 4. The computed phase field solution ϕ and a tanh profile generated using sharp interface solution.

We note that for even higher values of w, the bending energy contribution starts to diminish. We then are left with a singular perturbation problem since the zero bending energy case leads to the well known contact problem associated with the Laplace–Young law and an appropriate contact angle condition. For the latter case, it is possible to implement a more straightforward phase field model based on the phase field function and its low order gradient like the surface area functional $B = B(\phi)$, which would be more effective computationally than the higher order phase field energy functional established here for the bending energy. Our focus, in this work, is to consider situations where the bending energy plays an important role in the total energy contributions.

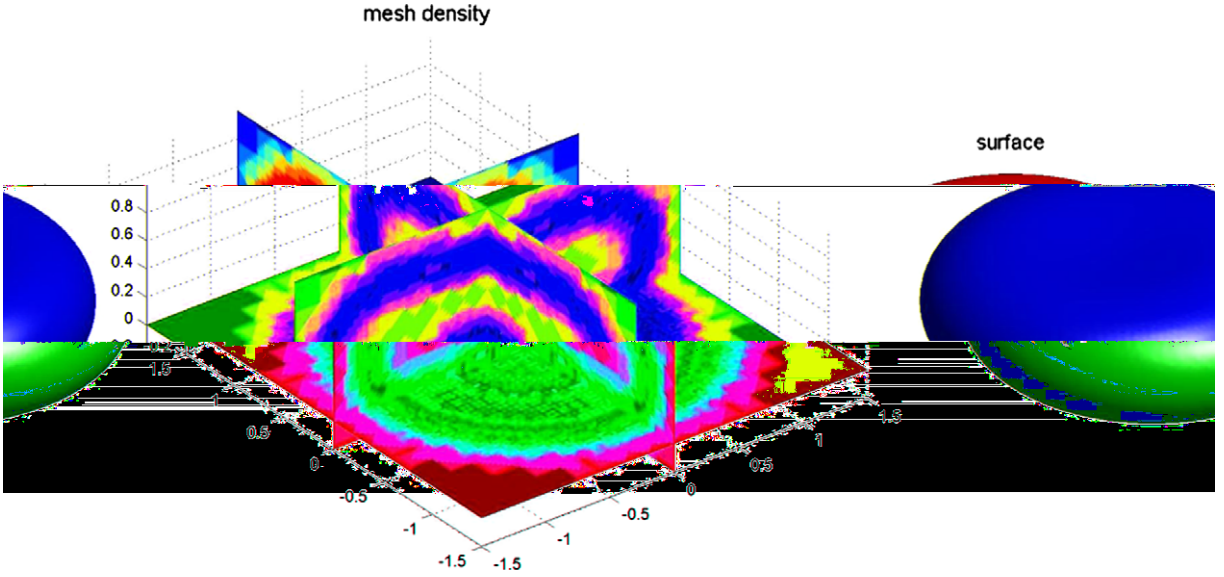

Fig. 5. Slices of the mesh density (left) and vesicle surface (right) for the phase field solution with $w = 1$.

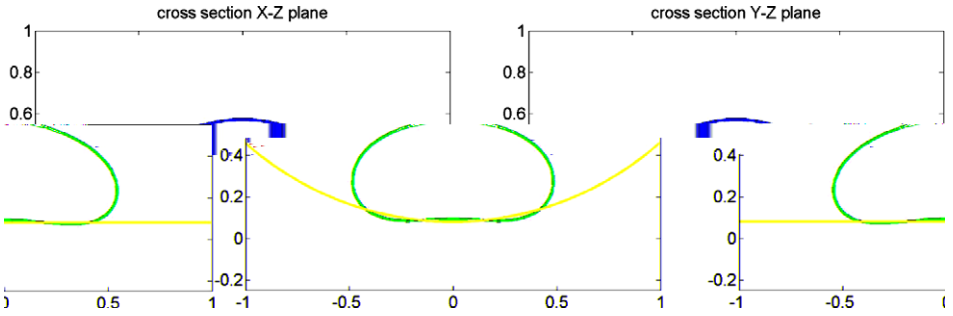

Fig. 6. The transverse cross section (left) and the section along the cylinder axis (right) of a non-axisymmetric solution with a cylindrical substrate of cross section radius 1.52, $w = 20, \epsilon = 0.02$ and $\delta = 0.15$.

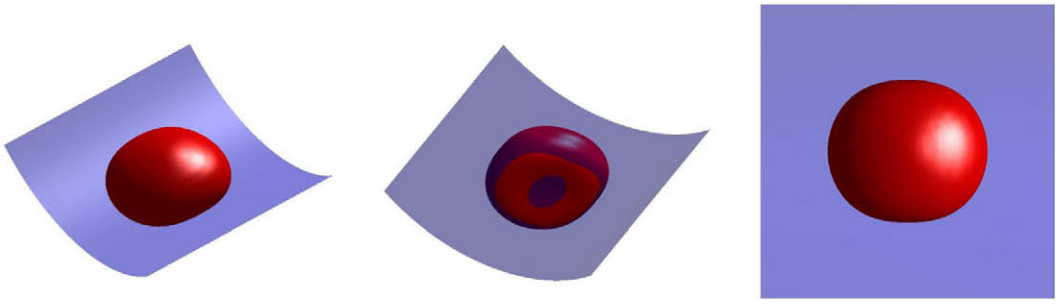

Fig. 7. 3D views of non-axisymmetric solution of Fig. 6 from different view angles. Left: viewed from above the substrate. Middle: viewed from below the substrate, the approximate annulus region is exhibiting the contact of the vesicle surface with the substrate; Right: viewed from top.

The cross sections of the vesicles for $w = 5$ and $w = 10$ are shown in Figs. 2 and 3, respectively, with the solutions for phase field model drawn in solid line and sharp interface model in dashed line.

The phase field solution ϕ is defined on the computational domain whose zero level set represents the vesicle surface Γ. We expect ϕ approaches a tanh profile

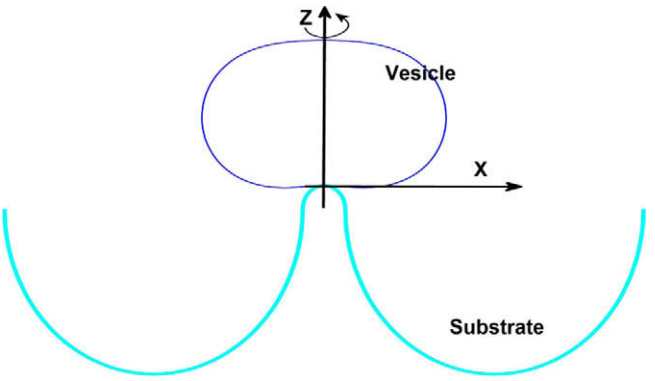

Fig. 8. Vesicle attached to the top of a substrate (the surface corresponding to the revolution of the curve shown in the lower half). The same vesicle but attached to the bottom of the substrate is shown in Fig. 9.

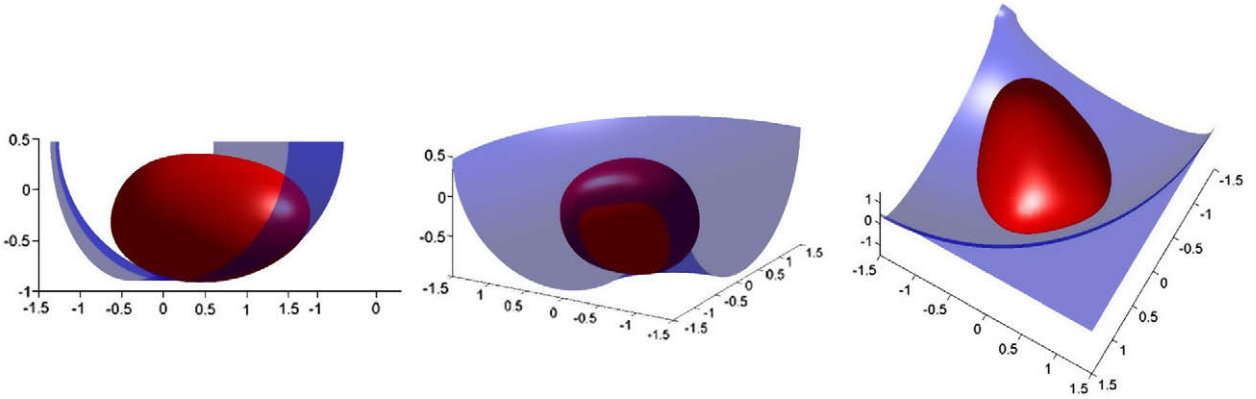

Fig. 9. Non-axisymmetric solution when the substrate is a cylindrical well generated by rotating a semi-circle (in x–z plane) of radius 1.4 about an axis parallel to z-axis (see Fig. 8). The minimum distance of the axis of rotation from the semi-circle is 0.2 unit. Other parameters are $w = 20, \epsilon = 0.02, \delta = 0.15$, surface area = 9.01, and volume =2.32. Left: a side view. Middle: viewed from below the substrate. The light red patch is showing the area of the vesicle in contact with the inner part of the substrate. Right: viewed from top.

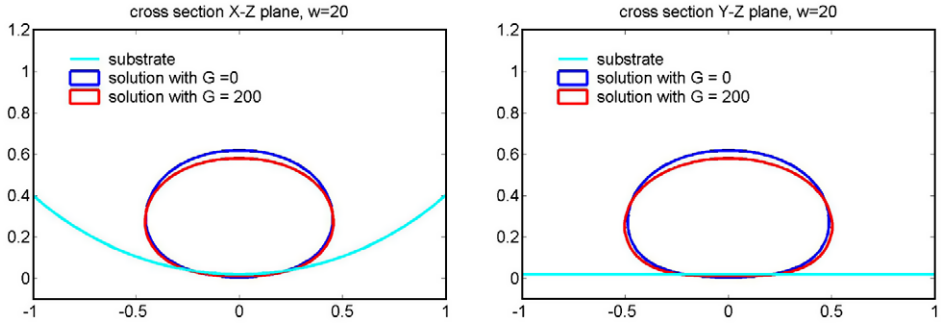

Fig. 10. The transverse cross section (left) and the section along the cylinder axis (right) of non-axisymmetric solutions with and without the gravitational energy, for a cylindrical substrate with cross section of radius 1.58, $w = 20, \epsilon = 0.02$ and $\delta = 0.1$.

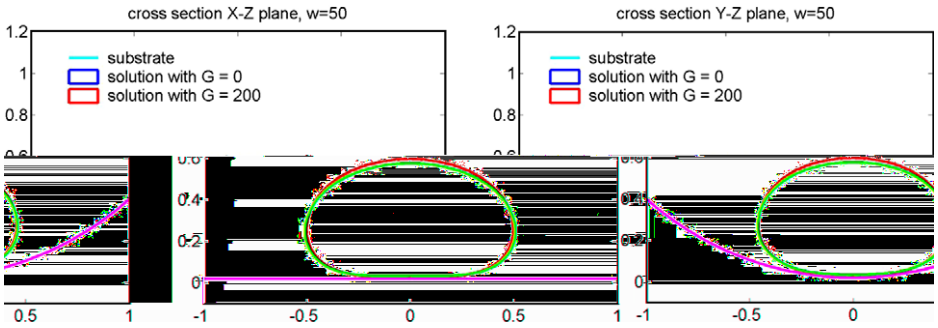

Fig. 11. The transverse cross section (left) and the section along the cylinder axis (right) of non-axisymmetric solutions, with and without the gravitational energy, for a cylindrical substrate with cross section radius 1.58, $w = 50, \epsilon = 0.02$ and $\delta = 0.1$.

$$\phi(x) \to \tanh\left(\frac{d(x,\Gamma)}{\sqrt{2}\epsilon}\right), \tag{14}$$

as $\epsilon \to 0$, where $d(x,\Gamma)$ is the signed distance from a point x to Γ. For $w = 1$ and $\delta = 0.15$, we used the sharp interface solution to generate a tanh profile as in (14) and compared it with the phase field solution ϕ computed using $\epsilon = 0.04$. Fig. 4 shows the two profiles restricted on the line $x = 0, y = 0$. The phase field function ϕ is seen to be very close to the tanh profile.

In addition, we plotted some sliced view of the mesh density and the shape of the computed vesicle in Fig. 5. The color coding reflects the mesh density, and it shows a much higher concentration of the mesh in the interfacial layer and thus signals the effectiveness of the adaptivity based on the *a posteriori* error estimation. We refer to [16] for more detailed benchmarks on the computational costs of the phase field model, in the absence of the adhesion term, with respect to different values of the diffuse interfacial width parameter ϵ. Much of the conclusions of [16] remain valid with the addition of the adhesion term.

5.2. Non-axisymmetric substrate

Notice that the substrate is built in the phase field model through a distance function, and it is easy to incorporate curved and non-axisymmetric substrate into the phase field model. To demonstrate this potential, we first look at an example of a cylindrical substrate, with the radius of the cylindrical cross section equal to 1.52. In this example, we set $\epsilon = 0.02, \delta = 0.15, w = 20$ and $G = 0$. Different views of the numerical solution are shown in Figs. 6 and 7.

In [11] we showed that concave-shaped axisymmetric substrates prefer adhesion more than convex or flat substrates. To explore the non-axisymmetric situation, we investigate the adhesion to a substrate obtained by revolving the curve shown in Fig. 8 (lower half). A vesicle shown there is attached to the top part of the substrate which is a convex spherical cap with radius 0.2. The substrate is formed by the top cap connected to a well which is the surface of revolution obtained by rotating a semi-circle of radius 1.4. The bending and adhesion energies for the vesicle are 14.80 and -5.55, respectively, when $w = 20$ and $\delta = 0.15$. When the vesicle attaches to the bottom (well) of the substrate, the symmetry is broken, and its shape can no longer be described by an axisymmetric computation. Fig. 9 shows the shape when the vesicle is attached to the bottom obtained by the phase field formulation developed in this paper. With $\epsilon = 0.02$ the solution has a bending energy valued at 16.37 and adhesion energy -67.49. The vesicle attaching to the bottom (non-axisymmetric in vesicle coordinate) has less total energy compared to the vesicle attaching to the top convex part, indicating that wells are favored for adhesion. This validates our earlier observation [11] that vesicles prefer concave substrates more for adhesion in the non-axisymmetric case, as well.

5.3. The effect of gravitational energy

Finally, we show an example where the gravitational energy (9) is added to the total energy. We take a cylindrical substrate with radius 1.58, and set the parameters as $\epsilon = 0.02, \delta = 0.1$, surface area =2.27 and volume =0.308. For comparison, we take two different cases of the contact potential with $w = 20$ and $w = 50$, and in each case, we consider the situation without the gravity effect ($G = 0$) and the one with $G = 200$ in the gravitational energy term. We note that the vesicles deform more under stronger gravitational force for both values of w and there is also more downward protrusion to the substrate (due to the heavier body). However, for stronger adhesion with $w = 50$ (Fig. 11), even though the deformation is still visible in the top portion of the vesicle, the protrusion effect is less significant, compared to the case of $w = 20$ (Fig. 10) with the same choice of $G = 200$. More phase field simulations can be carried out in the future to study the interplay between the gravity and the adhesion effect such as those in [21].

6. Conclusion

In this work, a phase field model is developed for the adhesion of a vesicle to substrates with various geometry. The model describes a general framework that can take into account the adhesion energy which depends on the proximity of the vesicle

with the substrate. While we consider the adhesion potential to be a Gaussian, any other form of the potential can be incorporated without further difficulty. The phase field model is solved in a 3D computational domain and requires, in general, more computational cost in comparison with the sharp interface description used for the axisymmetric analysis. To reduce the computational overhead, we employ an adaptive finite element method to compute solution of the phase field model so that most of the computational grids are mainly concentrated near the vesicle surface. We compute several axisymmetric shapes and compare with the sharp interface ODE solution for the validation of the model. Furthermore, we compute shapes for non-axisymmetric situations. The non-axisymmetric solutions obtained via phase field also supports the our earlier observations made in axisymmetric analysis that concave substrates favors adhesion. We also demonstrate that other energetic contributions, such as those due to gravitation effect, can also be properly incorporated in the phase field framework. The phase field approach developed here can also be extended to treat the adhesion of vesicles having free edges [28,36] based on the use of multiple phase field functions, similar to that discussed in [39]. Other possible extensions of our approach are the effect of mobile binders where the adhesive patch grows with time and the dynamics is dominated by intramembrane diffusion of binder molecules [7,34]. An adhesion potential that depend on the binder concentration and changes with time can be considered. Such generalizations as well as studies of the interaction of the GUVs with the substrate in a dynamic setting and with an external fluid environment will be considered in the future.

Acknowledgment

We would like to thank the referees for their valuable comments and suggestions of additional experiments and references.

References

[1] B. Alberts, A. Johnson, J. Lewis, M. Raff, K. Roberts, P. Walter, Molecular Biology of the Cell, fourth ed., Garland Science, NY, 2002.
[2] P. Atzberger, P. Kramer, C. Peskin, A stochastic immersed boundary method for fluid-structure dynamics at microscopic length scales, Journal of Computational Physics 224 (2007) 1255–1292.
[3] I. Babuska, T. Strouboulis, The Finite Element Method and Its Reliability, Oxford University Press, London, 2001.
[4] A.C. Balazs, Challenges in polymer science: controlling vesicle–substrate interactions, Journal of Polymer Science: Part B: Polymer Physics 43 (2005) 3357–3360.
[5] T. Biben, K. Kassner, C. Misbah, Phase-field approach to 3D vesicle dynamics, Physical Review E 72 (2005) 041921.
[6] M. Bloor, M. Wilson, Method for efficient shape parameterization of fluid membranes and vesicles, Physical Review E 61 (2000) 4218–4229.
[7] F. Brochard-Wyart, P.G. de Gennes, Adhesion induced by mobile binders: dynamics, PNAS 99 (2002) 7854–7859.
[8] F. Campelo, A. Hernandez-Machado, Dynamic model and stationary shapes of fluid vesicles, European Physical Journal E 20 (2006) 37–45.
[9] F. Campelo, A. Hernandez-Machado, Shape instabilities in vesicles: a phase-field model, European Physical Journal, Special Topics 143 (2007) 101–108.
[10] C. Carstensen, A posteriori error estimate for the mixed finite element method, Mathematics of Computation 66 (1997) 465–476.
[11] S.L. Das, Q. Du, Adhesion of vesicles to curved substrates, Physical Review E 77 (2008) 011907.
[12] Q. Du, C. Liu, R. Ryham, X. Wang, A phase field formulation of the Willmore problem, Nonlinearity 18 (2005) 1249–1267.
[13] Q. Du, C. Liu, X. Wang, A phase field approach in the numerical study of the elastic bending energy for vesicle membranes, Journal of Computational Physics 198 (2004) 450–468.
[14] Q. Du, C. Liu, X. Wang, Simulating the deformation of vesicle membranes under elastic bending energy in three dimensions, Journal of Computational Physics 212 (2006) 757–777.
[15] Q. Du, X. Wang, Convergence of numerical approximations to a phase field bending elasticity model of membrane deformations, International Journal of Numerical Analysis and Modeling 4 (2006) 41–459.
[16] Q. Du, J. Zhang, Adaptive finite element method for a phase field bending elasticity model of vesicle membrane deformations, SIAM Journal on Scientific Computation 30 (3) (2008) 1634–1657.
[17] A.J. Engler, S. Sen, H.L. Sweeney, D.E. Discher, Matrix elasticity directs stem cell lineage specification, Cell 126 (2006) 677–689.
[18] F. Feng, W. Klug, Finite element modeling of lipid bilayer membranes, Journal of Computational Physics 220 (2006) 394–408.
[19] C. Funkhouser, F. Solis, K. Thorton, Coupled composition–deformation phase-field method for multicomponent lipid membranes, Physical Review E 76 (2007) 011912.
[20] W. Helfrich, Elastic properties of lipid bilayers: theory and possible experiments, Zeitschrift fur Naturforschung 28c (1973) 693–703.
[21] M. Kraus, U. Seifert, R. Lipowsky, Gravity-induced shape transformations of vesicles, Europhysics Letters 32 (5) (1995) 431–436.
[22] D. Jamet, C. Misbah, Towards a thermodynamically consistent picture of the phase-field model of vesicles: local membrane incompressibility, Physical Review E 76 (2007) 051907.
[23] R. Lipowsky, E. Sackmann (Eds.), Structure and Dynamics of Membranes, Handbook of Biological Physics, vol. 1, Elsevier, Amsterdam, 1995.
[24] R. Lipowsky, U. Seifert, Adhesion of membranes: a theoretical perspective, Langmuir 7 (1991) 1867–1873.
[25] L. Ma, W. Klug, Viscous regularization and r-adaptive remeshing for finite element analysis of lipid membrane mechanics, Journal of Computational Physics 227 (2008) 5816–5835.
[26] J. McWhirter, G. Ayton, G. Voth, Coupling field theory with mesoscopic dynamical simulations of multi-component lipid bilayers, Biophysical Journal 87 (2004) 3242–3263.
[27] M. Meyer, M. Desbrun, P. Schröder, A. Barr, Discrete differential-geometry operators for triangulated 2-manifold, in: Proceedings of the VisMath, ACM, 2002.
[28] D. Ni, H. Shi, Y. Yin, Theoretical analysis of adhering lipid vesicles with free edges, Colloids and Surfaces B 46 (2005) 162–168.
[29] S. Rusinkiewicz, Estimating curvatures and their derivatives on triangle meshes, in: Proceedings of the 2nd International Symposium on 3D Data Processing, Visualization and Transmission, 2004 (3DPVT 2004), IEEE, 2004, pp. 486–493.
[30] E. Sackmann, Supported membranes: scientific and practical applications, Science 271 (1996) 43–48.
[31] U. Seifert, Adhesion of vesicles in two dimensions, Physical Review A 43 (1991) 6803–6814.
[32] U. Seifert, K. Berndl, R. Lipowsky, Shape transformations of vesicles: phase diagram for spontaneous curvature and bilayer-coupling models, Physical Review A 44 (2) (1991) 1182–1202.
[33] U. Seifert, R. Lipowsky, Adhesion of vesicles, Physical Review A 42 (1990) 4768–4771.
[34] V.B. Shenoy, L.B. Freund, Growth and shape stability of a biological membrane adhesion complex in the diffusion-mediated regime, PNAS 102 (2005) 3213–3218.
[35] P.S. Swain, D. Andelman, The influence of substrate structure on membrane adhesion, Langmuir 15 (1999) 8902–8914.

[36] Z. Tu, Z. Ou-yang, Lipid membranes with free edges, Physical Review E 68 (2003) 061915.
[37] R. Verfurth, A Review of a Posteriori Error Estimation and Adaptive Mesh-refinement Techniques, Wiley and Teubner, Chichester and Stuttgart, 1996.
[38] X. Wang, Asymptotic analysis of a phase field formulations of bending elasticity models, SIAM Journal on Mathematical Analysis 39 (2008) 1367–1401.
[39] X. Wang, Q. Du, Modeling and simulations of multi-component lipid membranes and open membranes via diffuse interface approaches, Journal of Mathematical Biology 56 (2008) 347–371.